Molecular Diversity (2021) 25:763–776
https://doi.org/10.1007/s11030-020-10054-w

ORIGINAL ARTICLE

Synthesis, characterization, antimicrobial, antioxidant and computational evaluation of *N*-acyl-morpholine-4-carbothioamides

Hamid Aziz[1] · Aamer Saeed[1] · Muhammad Aslam Khan[2] · Shakeeb Afridi[2] · Farukh Jabeen[3,4]

Received: 16 October 2019 / Accepted: 15 February 2020 / Published online: 25 February 2020

Abstract

The present research paper reports the convenient synthesis, successful characterization, in vitro antibacterial, antifungal, antioxidant potency and biocompatibility of *N*-acyl-morpholine-4-carbothioamides (**5a**–**5j**). The biocompatible derivatives were found to be highly active against the tested bacterial and fungal strains. Moreover, some of the screened *N*-acyl-morpholine-4-carbothioamides exhibited excellent antioxidant potential. Docking simulation provided additional information about possibilities of their inhibitory potential against RNA. It has been predicted by in silico investigation of the binding pattern that compounds **5a** and **5j** can serve as the potential surrogate for design of novel and potent antibacterial agents. The results for the in vitro bioassays were promising with the identification of compounds **5a** and **5j** as the lead and selective candidate for RNA inhibition. Results of the docking computations further ascertained the inhibitory potential of compound **5a**. Based on the in silico studies, it can be suggested that compounds **5a** and **5j** can serve as a structural model for the design of antibacterial agents with better inhibitory potential.

Graphic abstract

Binding mode of compound **5j** inside the active site of RNA in 3D space. **5j** displayed highest antibacterial potential than the reference drug ampicillin with ZOI 10.50 mm against *Staphylococcus aureus*. **5j** also displayed highest antifungal potential than the reference drug *amphotericin B* with ZOI 18.20 mm against *Fusarium solani*.

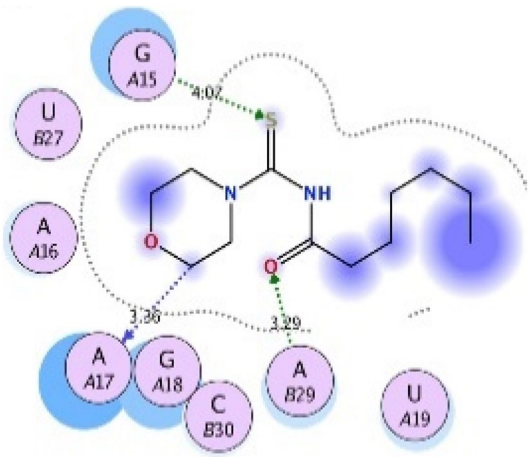

Electronic supplementary material The online version of this article (https://doi.org/10.1007/s11030-020-10054-w) contains supplementary material, which is available to authorized users.

Extended author information available on the last page of the article

Keywords Multidrug-resistant · Antibiotics · Antimicrobial · DNA · Disk diffusion

Introduction

The infectious diseases caused by drug-resistant microbial strains are a growing threat for scientific community to deal with [1]. Systemic and dermal fungal infections have been increased especially in immuno-suppressed individuals like cancer and AIDS [2]. Moreover, the available antifungal drugs being biochemically like human cells are associated with severe side effects. Another major problem is the lack of development of antibacterial agents against drug-resistant bacterial pathogens [3, 4]. Except for lipopeptides, most of the currently used antibiotics belong to those discovered before 1980s. Besides, most of the advances that have been made since 1980s are achieved through modifications to the existing antibiotics. Consequently, research has been focused toward the development of potent antimicrobial agents against novel targets to overcome the problems associated with the drug resistance [5, 6]. Accordingly, the development of potent antimicrobial agents or the expansion of previous antimicrobial drugs is required. In this regard, literature survey reveals thiourea-based heterocyclic analogues as potent and biocompatible antimicrobial agents [7].

Thioureas (TU) are organosulfur compounds having general formula of SC $(NH_2)_2$. These are versatile building blocks for the synthesis of biologically relevant heterocycles [8, 9]. The presence of hard O- and N- and soft S-donor atoms impart TU the ability to develop efficient H-bonding interactions. The H-bonding ability of TU has been exploited in the construction of anion receptors, metal complexes and organocatalysts [10]. The presence of electron-donating or electron-withdrawing groups imparts TU derivative electrochemical properties [8]. Aroyl TU are successfully employed in environmental control, as ionophores and in ion selective electrodes [11, 12]. In synthetic chemistry, TU derivatives are used in the synthesis of triazines, isoxazoles and oxazoles [13, 14]. TU have received central interest in recent past owing to their pharmacological activities like antidiabetic, antituberculosis, anti-inflammatory, insecticidal, rodenticidal, antiviral and antimicrobial [15]. A plethora of examples from the literature are available emphasizing the antibacterial and antifungal potential of TU derivatives. Quinazolinone-based TU possess analgesic, anticonvulsant, analgesic, cytotoxic and antimicrobial activities [16, 17]. TU incorporating a hippuric acid moiety exhibit antimicrobial activity comparable to the reference standard ciprofloxacin [18]. 5,5-Diphenylpyrrolidine *N*-aroylthiourea heterocycles display a broader spectrum of superior antibacterial and antimycobacterial activity [19]. Cui et al. reported the synthesis and antibacterial potential of thiouracil-based thioureas. The synthesized thioureas displayed good inhibitory potential against the tested bacterial strains [20]. TU derivatives such as thiophene-ethyl thiourea exhibited more efficient effects on multidrug-resistant HIV-1 strains than the standards commonly used such as trovirdine, delavirdine, MKC-442 and AZT [21]. Some literature-reported potent, biocompatible, antioxidant and antimicrobial thiourea is shown in Fig. 1.

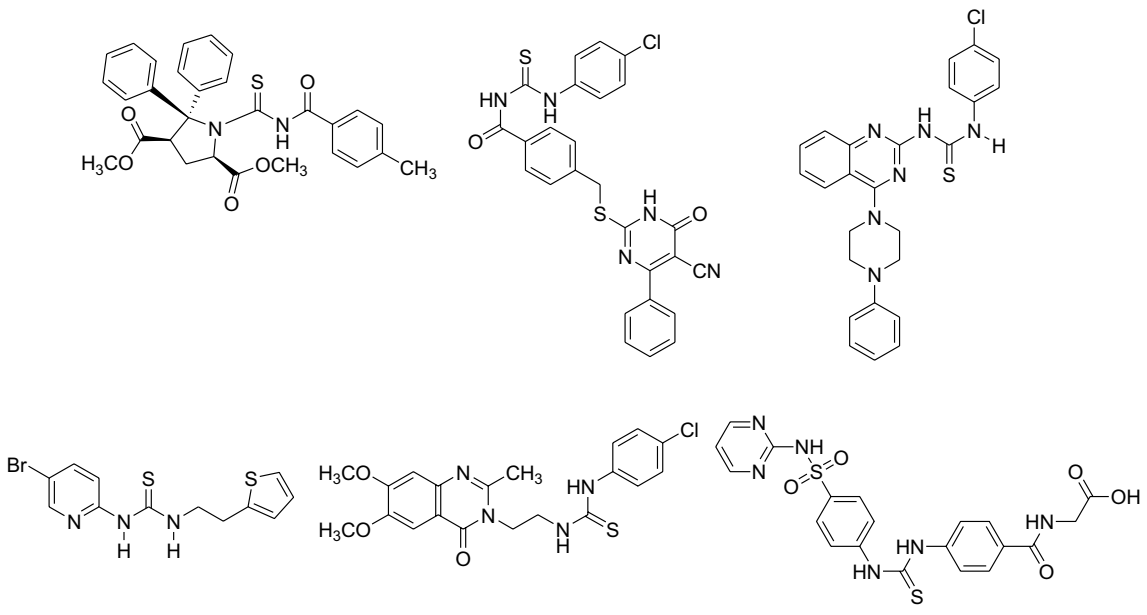

Fig. 1 Some literature-reported potent, biocompatible, antioxidant and antimicrobial thiourea derivatives

Considering the global spread of antibiotic resistance and the emergence of novel antibiotics-resistant microbes coupled with the lack of effective antibiotics, there is an urgent need for the design and synthesis of potent antimicrobial agents. In this context, the current research presents the facile synthesis, antimicrobial evaluation and docking analysis of some morpholine-based TU derivatives. The synthetic work proceeds in the presence of dry distilled acetone with higher yields.

Table 1 Synthesis of different *N*-acyl-morpholine-4-carbothioamide (**5a**–**5j**) derivatives

S. no.	Compound	*R*	S. no.	Compound	*R*
1	**5a**	2-NO_2Ph	6	**5f**	2-CH_3Ph
2	**5b**	Hydrogen atom (H)	7	**5g**	C_3H_7
3	**5c**	3-NO_2 Ph	8	**5h**	C_4H_9
4	**5d**	2,4-diClPh	9	**5i**	$PhCH_2$
5	**5e**	4-CH_3Ph	10	**5j**	C_6H_{13}

Results and discussion

Synthesis

The synthetic route adopted for the synthesis of *N*-acyl-morpholine-4-carbothioamides (**5a**–**5j**) derivatives is shown in Scheme 1. Briefly, aryl and alkyl chlorides (**2a**–**2j**) are synthesized from variously substituted acid derivatives at room temperature using dry DMF and thionyl chloride. The freshly obtained acid chlorides were added to a solution of potassium thiocyanate in dry distilled acetone to prepare corresponding aroyl/alkyl isothiocyanates (**3a**–**3j**). The latter were treated in situ with morpholine in equimolar ratios to furnish the corresponding the *N*-acyl-morpholine-4-carbothioamide (**5a**–**5j**) derivatives in excellent yields (70–90%). The synthesized compounds (**5a**–**5j**) (Table 1) were purified by recrystallization using DCM as a solvent at room temperature [9, 15].

Spectroscopic characterizations

Structures of the synthesized *N*-acyl-morpholine-4-carbothioamide (**5a**–**5j**) derivatives were assigned from spectroscopic technique (FT-IR, $^1H/^{13}C$ NMR) and elemental analysis (CHNS). The synthesized *N*-acyl-morpholine-4-carbothioamide (**5a**–**5j**) derivatives provided satisfactory elemental analysis results for the elements C, H, N and S aligned with the proposed structural formulae. FT-IR spectra displayed broader peaks for the NH protons at 3259.53–3339.75 cm^{-1} (SI Figs. 5, 9). The ^1H NMR spectra present peaks for NH protons at 8.60–8.48 ppm (SI Figs. 6, 10). FT-IR spectra have new peaks ranging from 1662.19 to 1683.90 cm^{-1} for the amide linkages (SI Figs. 5, 9). ^{13}C NMR spectra of the synthesized *N*-acyl-morpholine-4-carbothioamide (**5a**–**5j**) derivatives display sharp signals at 161–163 ppm for the resulting carbonyl carbon of the amides (SI Figs. 8, 12). ^1H NMR spectra display double doublets at 7.75–7.29 ppm for the 1,4-substituted pattern of the synthesized *N*-acyl-morpholine-4-carbothioamide (**5a**–**5j**) derivatives (SI Fig. 11). The aliphatic chain displays strong absorption peaks in the range of 2995–2867 cm^{-1} in the FT-IR spectra. The aliphatic chain display multiplets at 2.19–0.90 and 13–38 ppm in the ^1H and ^{13}C NMR spectra, respectively. The characteristic peak for thiocarbonyl carbon (C=S) is present as intense peak at 1259–1264 (SI Figs. 5, 9) in the FT-IR and at 177–179 ppm in ^{13}C NMR spectra (SI Figs. 8, 12) of the synthesized compounds.

In vitro antimicrobial assays

Antibacterial assay

The antibacterial potential of the synthesized *N*-acyl-morpholine-4-carbothioamide (**5a**–**5j**) derivatives was assessed from agar disk diffusion method using two gram-positive (*Staphylococcus aureus* and *Bacillus subtilis*) and three gram-negative (*Pseudomonas aeruginosa*, *Escherichia*

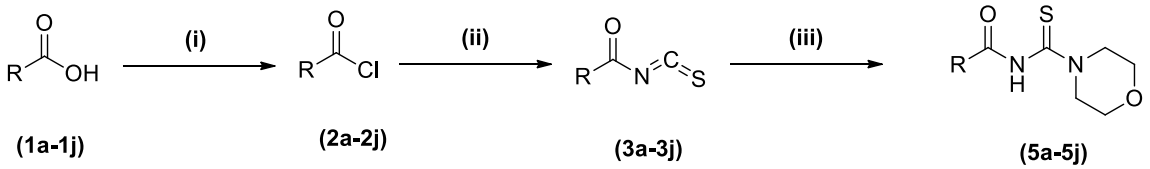

(1a-1j) (2a-2j) (3a-3j) (5a-5j)

(i). $SOCl_2$, DMF, 30 minutes stirring, 50 °C. **(ii).** KSCN, dry acetone, 30 minutes stirring, 50 °C

(iii). Morpholine, dry acetone

Scheme 1 Synthetic route employed for the synthesis of *N*-acyl-morpholine-4-carbothioamide (**5a**–**5j**) derivatives

coli and *Klebsiella pneumoniae*) strains. The antibacterial potential of the screened derivatives in terms of their zone of inhibition (ZOI) at a moderate concentration of 70 µg/disk is summarized in Table 2. The screened derivatives showed varied response against the various screened bacterial strains. Among the tested strains, the screened derivatives (**5a**–**5j**) were found to be more active against gram-positive bacterial strains than the gram-negative strains. The screened derivatives displayed highest potential against *Staphylococcus aureus* with **5j** and **5a** inducing the highest ZOI, i.e., 10.50 mm and 9.90 mm higher than the reference drug ampicillin. The same trend was found among the derivatives screened against *Bacillus subtilis* with **5j** and **5a** inducing the highest ZOI, i.e., 11.20 mm and 9.0 mm. In the case of gram-negative bacterial strains, *Pseudomonas aeruginosa* was found to be more resistant to the screened derivatives with highest ZOI displayed by **5j** and **5i**. However, derivatives **5c**, **5e** and **5f** were lacking any antibacterial potential. Moreover, the *Escherichia coli* were comparatively more prone to the screened derivatives where the compounds displayed highest antibacterial potential than the rest of the gram-negative bacterial strains. The screened derivative **5f** displayed the highest ZOI, i.e., 8.20 mm followed by **5j** and **5b** with almost similar ZOI, i.e., 8.0 mm. Furthermore, **5e** was found to be the least active derivative with no activity against *Pseudomonas aeruginosa* and *Klebsiella pneumoniae*.

Antifungal assay

The synthesized *N*-Acyl-morpholine-4-carbothioamide (**5a**–**5j**) derivatives were further evaluated to confer their antifungal potential against spore-forming strains via agar disk diffusion method. The results obtained are summarized in Table 3. Among the screened compounds, **5j** was found to be the most potent against the tested fungal strains as the most prominent zones of inhibition were observed against *Fusarium solani*, i.e., 18.20 mm higher than the reference drug amphotericin B at moderate concentration of 70 µg/disk. Derivative **5j** was found to be highly active against the remaining fungal strains with ZOI close to the standard reference drug used. Compound **5a** was found to be the most active one against *Aspergillus niger* with ZOI higher than amphotericin B. In general, *Aspergillus flavus* was found to be the slightly resistant strain against the screened strains. Derivative **5b** was

Table 3 Antifungal activity of the screened *N*-acyl-morpholine-4-carbothioamide (**5a**–**5j**) derivatives

S. no.	Compound	Zone of inhibition (in mm at 70 ug/disk)		
		A. flavus	*A. niger*	*F. solani*
1	**5a**	10.1	17.7	12.1
2	**5b**	7.1	8.0	5.8
3	**5c**	–	7.0	–
4	**5d**	6.0	7.9	7.0
5	**5e**	7.5	6.9	8.0
6	**5f**	6.2	5.8	6.1
7	**5g**	9.5	9.1	9.2
8	**5h**	10.3	10.1	11.3
9	**5i**	5.8	5.8	5.9
10	**5j**	12.6	10.3	18.2
11	**Amphotericin B**	15.6	16.0	15.4
12	**DMSO**	–	–	–

The sample concentration was 70 µg/mL. Values (mean ± SD) are average of triplicate

– no observed/calculated activity, *DMSO* negative control

Table 2 Antibacterial activity of the screened *N*-acyl-morpholine-4-carbothioamides (**5a**–**5j**) derivatives

S. no.	Compound	Zone of inhibition (mm)				
		E. coli	*P. aeruginosa*	*S. aureus*	*B. subtilis*	*K. pneumoniae*
1	**5a**	7.2	8.70	9.9	9.0	8.0
2	**5b**	8.0	6.20	8.0	6.0	5.3
3	**5c**	7.0	–	6.7	5.8	7.5
4	**5d**	6.9	7.50	7.8	9.5	8.0
5	**5e**	6.8	–	6.2	5.8	–
6	**5f**	8.2	–	7.0	6.9	5.3
7	**5g**	7.5	7.50	8.8	8.0	7.0
8	**5h**	6.9	8.0	9.7	8.0	8.3
9	**5i**	6.5	9.20	6.0	5.8	8.4
10	**5j**	8.0	13.0	10.5	11.2	9.5
11	**Ampicillin**	20	35.0	9.8	35	22
12	**DMSO**	–	–	–	–	–

The sample concentration was 70 µg/mL. Values (mean ± SD) are average of triplicate

– no observed/calculated activity, *DMSO* negative control

found to be inactive against the *Aspergillus flavus* and *Fusarium solani* and did not induce any prominent zone of inhibition.

Antioxidant assays

Total antioxidant capacity (TAC), total reducing power (TRP) and DPPH free radical scavenging assays were performed to probe the antioxidant potential of the synthesized compounds at a screening concentration of 200 µg/mL. TAC is based on the conversion of Mo (VI) to Mo (V) and indicates the quenching ability of the tested substance toward ROS [22]. In general, the screened compounds displayed varied antioxidant ability. Maximum value for total antioxidants in terms of ascorbic acid equivalents of the test compound was found as 123.47 ± 1.20 µg AAE/mg for compound **5i** followed by **5h**, **5f** and **5j** with TAC of 119.82 ± 1.21 µgAAE/mg, 112.63 ± 1.14 µgAAE/mg and 107.21 ± 0.82 µgAAE/mg, respectively. Furthermore, to assess the antioxidant capacity of the synthesized compounds TRP was performed. A compound possessing redox property neutralizes and absorbs free radicals by transformation of Fe^{+3} to Fe^{+2} ion. Compounds possessing reducing power have the capacity to reduce ferric ion into ferrous ion [23]. Highest reducing power potential was observed for **5i** as 158.71 ± 0.40 µgAAE/mg followed by **5f**, **5g**, **5j** as 141.47 ± 0.64 µgAAE/mg, 132.46 ± 0.22 µgAAE/mg and 129.51 ± 1.0 µgAAE/mg, respectively. Subsequently, DPPH free radical scavenging assay was performed to augment the TAC and TRP. The spectrophotometric method is based on quenching of stable colored radicals of DPPH indicating the scavenging ability of antioxidants [24]. Likewise, free radical scavenging activity varied among the compounds with some exhibited excellent scavenging potential. Significant FRSA was observed for **5f** and **5i** with 64.21 ± 0.32% and 58.81 ± 0.44 at 200 µg/mL with IC_{50} 154 µg/mL and 180 µg/mL, respectively. From the results summarized, it can be suggested that compounds **5f**, **5i**, **5g** and **5j** exhibited excellent antioxidant potential and have the potential to be further analyzed for in vivo antioxidant potency (Table 4).

Biocompatibility against human red blood cells (hRBCs)

To evaluate the biosafe nature, the synthesized *N*-acyl-morpholine-4-carbothioamide (**5a**–**5j**) derivatives were screened for biocompatibility against human red blood cells (hRBCs). In the experiment, freshly isolated human red blood cells (hRBCs) and test compounds were co-incubated in phosphate buffer saline (PBS) that mimic extracellular environment [25]. The bioassay is based on the release and measurement of hemoglobin from red blood cells (RBCs) which can be prompt by the tested compound if it could rupture RBCs [26]. The compounds were tested for hemolytic activity at high concentration, i.e., 400 µg/mL. In generally, hemolysis ≥ 25% is considered hemolytic, while hemolysis ≤ 10% is considered non-hemolytic. In the study, the tested compounds exhibited remarkable hemocompatibility even at the highest concentration as shown in Table 5. The study thus concludes that the synthesized compounds are highly compatible; however, detailed in vivo studies are required to verify and augment the in vitro results.

Molecular docking

Molecular docking analysis was opted to get deeper insights into the RNA binding affinity in silico for the screened compounds. In order to study the binding interaction of the series of synthesized compounds, investigators relied on molecular docking simulations to complement the experimental results and to acquire the binding mode [27–31]. The volume occupied by the cognate ligand in the receptor was defined as the binding site of the minimized eubacterial ribosomal

Table 4 Antioxidant potential of the screened *N*-acyl-morpholine-4-carbothioamide (**5a**–**5j**) derivatives at 200 µg/mL

S. no.	Compound	TAC (µg AAE/mg)	TRP (µg AAE/mg)	DPPH (% FRSA)	DPPH (IC_{50}) µg/mL
1	**5a**	91.66 ± 1.14	121.32 ± 1.24	33.5 ± 1.38	> 200
2	**5b**	73.71 ± 1.32	96.71 ± 0.98	28.11 ± 1.2	> 200
3	**5c**	52.43 ± 0.84	74.23 ± 0.92	23.32 ± 1.74	> 200
4	**5d**	81.72 ± 0.71	93.87 ± 0.95	27.0 ± 0.97	> 200
5	**5e**	86.78 ± 1.22	93.23 ± 1.13	29.37 ± 1.22	> 200
6	**5f**	112.63 ± 0.22	141.47 ± 0.64	58.81 ± 0.44	180
7	**5g**	97.23 ± 1.13	132.46 ± 0.22	51.33 ± 0.82	200
8	**5h**	119.82 ± 1.32	152.91 ± 1.43	53.85 ± 0.71	200
9	**5i**	123.47 ± 1.20	158.71 ± 0.40	64.21 ± 0.32	154
10	**5j**	107.21 ± 1.43	129.51 ± 1.0	50.93 ± 0.47	200

Values (mean ± SD) are average of triplicate

Table 5 % Hemolysis of the screened *N*-acyl-morpholine-4-carbothioamide (**5a**–**5j**) derivatives

S. no.	Compound	% Hemolysis
1	**5a**	0.842 ± 0.22
2	**5b**	0.25 ± 0.18
3	**5c**	0.72 ± 0.20
4	**5d**	1.28 ± 0.22
5	**5e**	0.66 ± 0.24
6	**5f**	2.04 ± 0.08
7	**5g**	0.53 ± 0.12
8	**5h**	2.17 ± 0.22
9	**5i**	0.88 ± 0.38
10	**5j**	0.72 ± 0.12
11	**DMSO**	0.19 ± 0.08

The sample concentration was 400 µg/mL. Values (mean ± SD) are average of triplicate

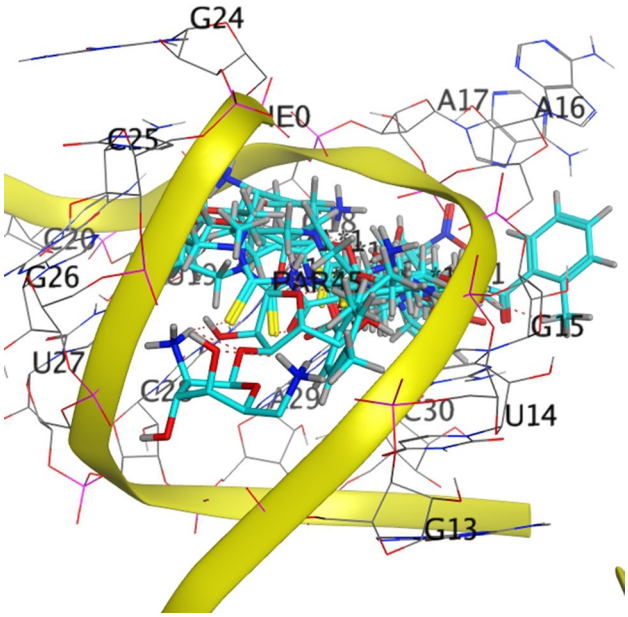

Fig. 2 Superimposition of docked ligands inside the active site of RNA. Ligands are presented in thick tube mode, heteroatoms in elemental color and carbon in cyan color, while receptor is shown in ribbon format in yellow color, and bases are presented in wires. (Color figure online)

decoding A site (*E. coli* 16S rRNA A site) and an input site sphere was defined within a radius of 5 Å located inside the major groove of receptor. The ligands with optimized geometries were docked into the active site of the minimized eubacterial ribosomal decoding A site (*E. coli* 16S rRNA A site, PDB codes:1j7t). van der Waals forces, H bonds, electrostatic and hydrophobic interactions are the acting forces found between a small molecule and macromolecule found to anchor the ligands within the gorge of active site. The variants with receptor–inhibitor complex having lowest energy were selected, for further studies. Among the docked conformations for each ligand, the most favorable conformation was retained to perform further analysis of the interactions. Docking poses having lowest binding energy, and a maximum number of docking interactions were ranked as the most favorable pose. The software computed their binding energy as a negative value. The most preferred docking poses among all the docked conformations was used to probe the interactions of the docked conformations with the nitrogen bases.

Consequently, the screened compounds were found to be nicely stacked within the active site of the major groove of the RNA complex (Fig. 2). H-bonding significantly influences the binding of the screened compounds with RNA. Detailed investigation of the interaction of screened compounds with the RNA duplex of RNA was performed. The docked poses of the screened compounds were observed to be significantly surrounded by nitrogen bases A16, A17, A29, C30, G15, G18, U19 influencing the interaction and in turn driving inhibitory potential of the antibacterial compounds. Based on the observations, the carbonyl oxygen of the screened compounds was found to have displayed H-bonding with the key nitrogen bases and anchored the molecular geometries within the active site. This H-bonding displayed by the screened compounds is responsible for imparting stability to the screened compounds inside the pocket of RNA.

The docked compounds showed sufficiently strong interactions especially, **5a** which was stabilized by H-bonding with the key bases including A17 and C30. Ligand **5a** also formed π–H interaction which provided further strength inside the major groove of RNA. Similarly, compound **5j** was anchored inside the RNA pocket via tremendous significant H-bonding and aromatic H-bonding with the nitrogen bases. Figure 3a, b shows binding pattern of the compound inside the major groove of the duplex. Ligand **5j** stabilized itself in the binding pocket by establishing copious electrostatic contacts with the nitrogen bases including hydrogen bonding, G15, A31, A17 (Fig. 4a, b) and aromatic H-bonding, C30. Moreover, ligands **5a** and **5j** showed good binding energy, − 8.54 kCal/mol and − 8.52 kCal/mol further ascertain the strong binding and inhibitory potential of ligands **5a** and **5j**.

The docked ligands exhibited fairly well binding with energy values ranging from − 9.62 to − 7.63 KCal/mol. The higher binding energy values stabilized the ligands within the gorge of the active site through various interactions with RNA pocket. The lowest energy docked poses was associated with significant binding features mainly based on interaction due to numerous interacting moieties of the druglike ligands including the versatile structure of the docked ligands.

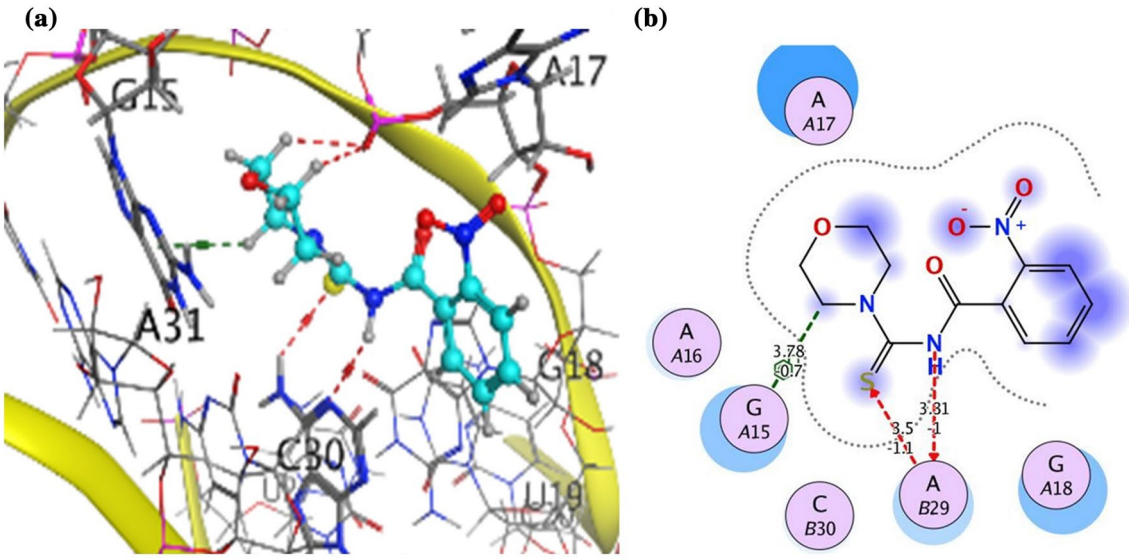

Fig. 3 Binding mode of compound **5a** inside the active site of RNA in 3D space. **a**, **b** Docking poses of compound **5a** in 3D space. Ligands are presented in thick tube mode with elemental and cyan color, while key residues are presented in wire mode, elemental color and the helix of duplex is shown in yellow-colored ribbon format. **a** Aromatic H-bonding and H-bonding of ligand atoms and bases. **b** Docked pose of ligand **5a** within the active site in 2D space. (Color figure online)

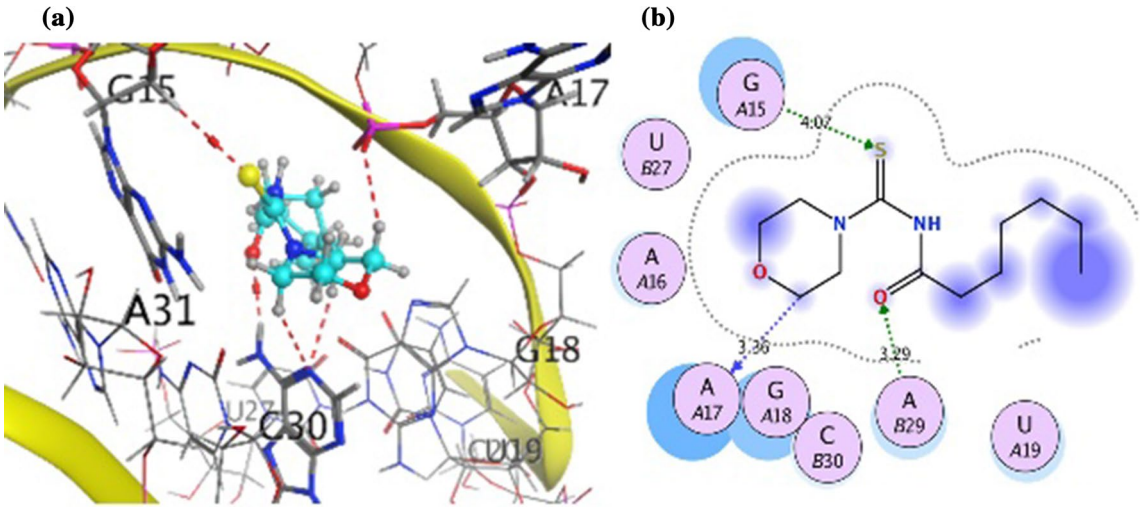

Fig. 4 Binding mode of compound **5j** inside the active site of RNA in 3D space. **a**, **b** 3D docked poses of compound **5j**. Ligand is presented in tube-and-ball mode in elemental and cyan color, interacting residues are shown in tube mode elemental color, while key residues are shown in wire mode, elemental color and the helix of duplex is shown in yellow-colored ribbon format. **a** H-bonding of ligand atoms and bases. **b** Docked pose of ligand **5j** within the active site in 2D space. (Color figure online)

Drug likeness

Descriptors such as number of rotatable bonds, hydrogen bond donor (NOR), hydrogen bond acceptor (HBA), Lipinski's acceptors (lip_acc), Lipinski's donors (lip_don), Lipinski's violation (lip_viol), Lipinski's drug likeness (lip_drug), log*P*, molecular weight and total polar surface area (TPSA) were computed to check the druglike properties of the synthesized *N*-acyl-morpholine-4-carbothioamide (**5a**–**5j**) derivatives. In silico results revealed the synthesized *N*-acyl-morpholine-4-carbothioamide (**5a**–**5j**) showed compliance to the Lipinski's Ro5 [32] and Veber's Ro3 [33], cutoff limits, which pave their way to be used as RNA inhibitors with no derivative found to show any violation.

Accordingly, the druglike molecules must have molecular weight ≤ 500, log *P* (logarithm of the octanol/water partition coefficient) ≤ 5, total polar surface area (TPSA) < 140 $Å^2$, number of hydrogen bond donors (HBD) ≤ 5 and hydrogen

bond acceptor (HBA) ≤ 10 as per Lipinski's Ro5 [32]. Veber et al. offered further modifications in the Ro5 [33]. According to Veber, number of rotatable bonds (NOR) of a druglike molecule should be fewer or equal to 10 [32]. Molecules may have problem with bioavailability, which violate more than one of these criteria. Detailed results of drug likeness of the *N*-acyl-morpholine-4-carbothioamides (**5a**–**5j**) are tabulated in Table 6.

Conclusions

The present paper presents the synthesis of a series of *N*-acyl-morpholine-4-carbothioamide (**5a**–**5j**) derivatives. The synthesized compounds were investigated against pathogenic bacterial and fungal strains. Our results concluded that the compounds exhibited excellent growth inhibitory potential against gram-positive and gram-negative bacteria as well as against certain spore-forming fungi. Antioxidant studies revealed that some of the derivatives such as **5i** and **5f** possess considerable antioxidant properties. Moreover, the derivatives were found to be highly hemocompatible that make the derivatives biosafe. To ascertain the possible influence of inhibitory potential of compounds, molecular docking was performed. On the basis of docking computations, compounds **5a** and **5j** showed good binding mode. Thus, we suggest that the electrostatic and hydrophobic interactions existing between the target and compounds, particularly **5a** and **5j**, are well corroborated by the experimental data. Docking simulation also elucidated the valuable information to understand the mechanistic pathway of inhibition and can contribute to the molecular design and synthesis of potent antibacterial and fungal agents to quite a good level. These results further demonstrate that compounds **5a** and **5j** can serve as the structural model for design of novel antibacterial agents.

Materials and methods

Experimental

The reactions involved were performed in a flame-dried glassware under a positive pressure of nitrogen gas using dry distilled solvents. Dried and purified commercial-grade solvents and reagents were purchased directly from chemical suppliers and were used without any further purification. Thin-layer chromatography was performed using silica gel 60 F254 precoated plates (0.25 mm) to judge the progress of the reaction by TLC analysis (single spot/two solvent systems) using UV lamp for detection purposes. ^{1}H and ^{13}C NMR spectra were recorded on a 400 and 100 MHz Bruker Avance AVIII spectrometer for compounds **5a**–**5j** except compound **5f**, where ^{1}H and ^{13}C NMR spectra were recorded on a 300 and 75 MHz Bruker spectrometer. TMS was used as an internal standard and deuterated chloroform ($CDCl_3$) as a solvent for compounds **5a**–**5j** except compound **5f**, where deuterated acetone was used. Proton chemical shifts are reported as δ values in ppm relative to residual signals from deuterated solvents, while coupling constants are indicated by *J* in Hz. PerkinElmer spectrum 1000 series Fourier transform infrared ATR spectrometer was used to record the infrared spectra, and the spectra are measured in wave numbers (cm^{-1}). The synthesized compounds were subjected to elemental analysis to determine % of each element.

Synthesis of *N*-acyl-morpholine-4-carbothioamide (5a–5j)

The synthetic work was accomplished as reported elsewhere, but with minor modifications. Briefly, acid chlorides were synthesized from substituted acid derivatives (10 mmol) and thionyl chloride (10 mmol) at 50 °C using dry DMF as a catalyst. The freshly prepared acid chloride (10 mmol) dissolved in dry distilled acetone (10 mL) was added dropwise

Table 6 Physicochemical descriptors of the *N*-acyl-morpholine-4-carbothioamide (**5a**–**5j**) derivatives

Code	HBA	HBD	NOR	h_pKb	lip_acc	lip_don	lip_drug	lip_viol	logP (o/w)	logS	TPSA	Weight
5a	3.00	1.00	3.00	14.00	7.00	1.00	1.00	0.00	0.78	−4.20	119.48	295.32
5b	3.00	1.00	2.00	14.00	4.00	1.00	1.00	0.00	0.84	−3.41	73.66	250.32
5c	3.00	1.00	3.00	14.00	7.00	1.00	1.00	0.00	0.82	−4.20	119.48	295.32
5d	3.00	1.00	2.00	14.00	4.00	1.00	1.00	0.00	2.06	−4.88	73.66	319.21
5e	3.00	1.00	2.00	14.00	4.00	1.00	1.00	0.00	1.14	−3.89	73.66	264.34
5f	3.00	1.00	2.00	14.00	4.00	1.00	1.00	0.00	1.14	−3.89	73.66	264.34
5g	3.00	1.00	3.00	14.00	4.00	1.00	1.00	0.00	0.10	−2.37	73.66	216.30
5h	3.00	1.00	4.00	14.00	4.00	1.00	1.00	0.00	0.54	−2.88	73.66	230.33
5i	3.00	1.00	3.00	14.00	4.00	1.00	1.00	0.00	0.93	−3.47	73.66	264.34
5j	3.00	1.00	6.00	14.00	4.00	1.00	1.00	0.00	1.43	−3.91	73.66	258.38

to a suspension of potassium thiocyanate (10 mmol) in acetone (05 mL), and the reaction mixture was refluxed at 50 °C for 30 min under nitrogen. After cooling to room temperature, a solution of the morpholine (10 mmol) in dry distilled acetone (10 mL) was added to the resulting mixture and was refluxed for 30 further min. After the required time, the reaction mixture was poured into cold water and the products precipitated were recrystallized from DCM [9, 15].

N-(2-Nitrobenzoyl)morpholine-4-carbothioamide (5a)

Mol. Wt. 327.31, Yield 76%, $R_f = 0.48$ (pet-ether: ethyl acetate 4:1), Yellow powder, m.p 130 °C. IR (ATR, cm^{-1}) ν: 3289.24 (NH), 2973.5 (sp^2 C–H), 2958.23, 2876.58 (sp^3 C–H), 1683.29 (NCO), 1601.37, 1580.19, 1519.60 (Ar–C=C), 1440.97 (–C–H bending), 1354.23 (–C–H bending), 1245.75 (C=S); ^{1}H NMR ($CDCl_3$): $\delta = 8.63$ (b, s, 1H, NH), 8.43 (d, 1H, $J = 8.29$ Hz, Ar–H), 8.24 (d, 1H, $J = 8.29$ Hz, Ar–H), 7.86 (t, 1H, $J = 8.2$ Hz, Ar–H), 7.79 (t, 1H, $J = 8.2$ Hz, Ar–H), 4.20 (b, s, 2H, O–CH_2), 3.85 (b, s, 4H, N–CH_2, O–CH_2), 3.76 (b, s, 2H, N–CH_2); ^{13}C NMR ($CDCl_3$): $\delta = 180.71$ (C=S), 169.83 (C=O), 147.24 (Ar), 135.43 (Ar), 133.40 (Ar), 128.34 (Ar), 128.13 (Ar), 121.24 (Ar), 66.34 (O–CH_2), 52.82 (b, N–CH_2), 52.24 (b, N–CH_2); Anal. Calc. for $C_{12}H_{13}N_3O_4S$: C: 48.81%; H: 4.44%; N: 14.23%; S: 10.86%; Found: C: 48.75%; H: 4.48%; N: 14.29%; S: 10.88%.

N-Benzoylmorpholine-4-carbothioamide (5b)

Mol. Wt. 282.0, Yield 80%, $R_f = 0.38$ (pet-ether: ethyl acetate 4:1), Light yellow powder, m.p 154 °C. IR (ATR, cm^{-1}) ν: 3237.48 (NH), 2970.84 (sp^2 C–H), 2924.72, 2848.35 (sp^3 C–H), 1663.62 (NCO), 1520.27, 1451.88, 1441.58 (Ar–C=C), 1425.58 (–C–H bending), 1357.40 (–C–H bending), 1222.82 (C=S); ^{1}H NMR ($CDCl_3$): $\delta = 8.46$ (b, s, 1H, NH), 7.83 (m, 2H, Ar–H), 7.60 (m, 1H, Ar–H), 7.49 (m, 2H, Ar–H), 4.24 (b, s, 2H, O–CH_2), 3.845 (b, s, 4H, N–CH_2, O–CH_2), 3.667 (b, s, 2H, N–CH_2); ^{13}C NMR ($CDCl_3$): $\delta = 179.23$ (C=S), 163.22 (C=O), 133.23 (Ar), 132.32 (Ar), 129.03 (Ar), 127.79 (Ar), 66.26 (O–CH_2), 52.80 (b, N–CH_2), 51.70 (b, N–CH_2); Anal. Calc. for $C_{12}H_{14}N_2O_2S$: C: 57.58%; H: 5.64%; N: 11.19%; S: 12.81%; Found: C: 57.55%; H: 5.63%; N: 11.21%; S: 12.85%.

N-(3-Nitrobenzoyl)morpholine-4-carbothioamide (5c)

Mol. Wt. 327.31, Yield 90%, $R_f = 0.48$ (pet-ether: ethyl acetate 4:1), m.p 146 °C; Yellow powder, IR (ATR, cm^{-1}) ν: 3350.65 (NH), 2958.73 (sp^2 C–H), 2962.75, 2866.98 (sp^3 C–H), 1676.39 (NCO), 1578.49, 1531.0 (Ar–C=C), 1409.67 (–C–H bending), 1384.24 (–C–H bending), 1239.18 (C=S); ^{1}H NMR ($CDCl_3$): $\delta = 8.56$ (b, s, 1H, NH), 8.93 (s, 1H, Ar–H), 8.48 (d, 1H, $J = 8.6$ Hz, Ar–H), 8.36 (d, 1H, $J = 8.6$ Hz, Ar–H), 7.79 (t, 1H, $J = 7.8$ Hz, Ar–H), 4.22 (b, s, 2H, O–CH_2), 3.86 (b, s, 4H, N–CH_2, O–CH_2), 3.75 (b, s, 2H, N–CH_2); ^{13}C NMR ($CDCl_3$): $\delta = 180.91$ (C=S), 169.63 (C=O), 148.54 (Ar), 135.14 (Ar), 133.64 (Ar), 129.34 (Ar), 124.58 (Ar), 122.44 (Ar), 66.30 (O–CH_2), 53.08 (b, N–CH_2), 52.14 (b, N–CH_2); Anal. Calc. for $C_{12}H_{13}N_3O_4S$: C: 48.81%; H: 4.44%; N: 14.23%; S: 10.86%; Found: C: 48.70%; H: 4.45%; N: 14.29%; S: 10.93%.

N-(2,4-Dichlorobenzoyl)morpholine-4-carbothioamide (5d)

Mol. Wt. 319.21, Yield 85%, $R_f = 0.42$ (pet-ether: ethyl acetate 4:1), m.p 136 °C, Yellow powder, IR (ATR, cm^{-1}) ν: 3259.53 (NH), 2985.49 (sp^2 C–H), 2930.628, 286.90 (sp^3 C–H), 1683.90 (NCO), 1582.82, 1526.52, 1456.94 (Ar–C=C), 1435.81 (–C–H bending), 1371.94 (–C–H bending), 1262.24 (C=S); ^{1}H NMR ($CDCl_3$): $\delta = 8.60$ (b, s, 1H, NH), 7.62 (d, 1H, $J = 8.4$ Hz, Ar–H), 7.476 (d, 1H, $J = 2.0$ Hz, Ar–H), 7.365 (dd, 1H, $J = 8.4$ Hz, Ar–H), 4.19 (b, s, 2H, O–CH_2), 3.84 (b, s, 4H, N–CH_2, O–CH_2), 3.72 (b, s, 2H, N–CH_2); ^{13}C NMR ($CDCl_3$): $\delta = 177.94$ (C=S), 161.37 (C=O), 138.39 (Ar), 132.15 (Ar), 131.62 (Ar), 131.34 (Ar), 130.55 (Ar), 127.85 (Ar), 66.21 (O–CH_2), 52.80 (b, N–CH_2), 51.54 (b, N–CH_2); Anal. Calc. for $C_{12}H_{12}Cl_2N_2O_2S$: C: 45.15%; H: 3.79%; N: 8.78%; S: 10.05%; Found: C: 45.05%; H: 3.89%; N: 8.83%; S: 10.0%.

N-(4-Methylbenzoyl)morpholine-4-carbothioamide (5e)

Mol. Wt. 264.34, Yield 79%, $R_f = 0.52$ (pet-ether: ethyl acetate 4:1), m.p 152 °C, White powder, IR (ATR, cm^{-1}) ν: 3339.75 (NH), 3031.0, 2962.12 (sp^2 C–H), 2924.34, 2866.24 (sp^3 C–H), 1662.19 (NCO), 1610.17, 1589.20, 1521.52, 1452.78 (Ar–C=C), 1428.95 (–C–H bending), 1389.94 (–C–H bending), 1259.47 (C=S); ^{1}H NMR ($CDCl_3$): $\delta = 8.48$ (b, s, 1H, NH), 7.31 (d, 2H, $J = 8.0$ Hz, Ar–H), 7.282 (d, 2H, $J = 8.0$ Hz, Ar–H), 4.23 (b, s, 2H, O–CH_2), 3.83 (b, s, 4H, N–CH_2, O–CH_2), 3.65 (b, s, 2H, N–CH_2), 2.431 (s, 3H, C–H); ^{13}C NMR ($CDCl_3$): $\delta = 179.41$ (C=S), 163.20 (C=O), 144.09 (Ar), 129.67 (Ar), 127.87 (Ar), 127.70 (Ar), 66.26 (O–CH_2), 52.80 (b, N–CH_2), 51.54 (b, N–CH_2), 21.639 (C–H); Anal. Calc. for $C_{11}H_8N_4O_3S$: C: 59.07%; H: 6.10%; N: 10.60%; S: 12.13%; Found: C: 59.01%; H: 6.11%; N: 10.63%; S: 12.16%.

N-(2-Methylbenzoyl)morpholine-4-carbothioamide (5f)

Mol. Wt. 264.34, Yield 70%, $R_f = 0.45$ (pet-ether: ethyl acetate 4:1), m.p 280 °C, White powder, IR (ATR, cm^{-1}) ν: 3259.45 (NH), 3044.09 (sp^2 C–H), 2896.16 (sp^3 C–H), 1634.08 (NCO), 1583.34, 1543.71 (Ar–C=C), 1430.55 (–C–H bending), 1363.91 (–C–H bending), 1281.21 (C=S);

^{1}H NMR (CD_3COCD_3): $\delta = 9.68$ (b, s, 1H, NH), 7.56 (d, 1H, $J = 7.50$ Hz, Ar–H), 7.41 (t, 1H, $J = 8.4$ Hz, Ar–H), 7.28 (m, 2H, Ar–H), 4.20 (b, s, 2H, O–CH_2), 3.78 (b, s, 6H, N–CH_2, O–CH_2), 2.90 (s, 3H, C–H); ^{13}C NMR (CD_3COCD_3): $\delta = 179.55$ (C=S), 165.75 (C=O), 136.93 (Ar), 134.60 (Ar), 130.99 (Ar), 130.71 (Ar), 127.81 (Ar), 125.60 (Ar), 65.93 (O–CH_2), 51.83 (b, N–CH_2), 50.87 (b, N–CH_2), 19.31 (C–H); Anal. Calc. for $C_{13}H_{16}N_2O_2S$: C: 59.07%; H: 6.10%; N: 10.60%; S: 12.13%; Found: C: 59.0%; H: 6.17%; N: 10.64%; S: 12.10%.

N-Butyrylmorpholine-4-carbothioamide (5g)

Mol. Wt. 216.30, Yield 80%, $R_f = 0.47$ (pet-ether: ethyl acetate 4:1), m.p > 300 °C, Light Yellow powder, IR (ATR, cm^{-1}) ν: 3290.85 (NH), 3091.05 (sp^2 C–H), 2964.81, 2852.11 (sp^3 C–H), 1716.34 (NCO), 1540.32, 1498.98, 1466.72 (Ar–C=C), 1444.72 (–C–H bending), 1371.96 (–C–H bending), 1246.27 (C=S); ^{1}H NMR ($CDCl_3$): $\delta = 8.32$ (b, s, 1H, NH), 4.15 (b, s, 2H, O–CH_2), 3.80 (b, s, 4H, N–CH_2, O–CH_2), 3.70 (b, s, 2H, N–CH_2), 2.19 (t, 2H, $J = 7.90$ Hz, C–H), 1.68 (sixtet, 2H, $J = 7.90$ Hz, C–H), 0.95 (t, 3H, $J = 7.90$ Hz, C–H); ^{13}C NMR ($CDCl_3$): $\delta = 180.47$ (C=S), 175.47 (C=O), 66.21 (O–CH_2), 52.70 (b, N–CH_2), 51.75 (b, N–CH_2), 38.44 (C–H), 19.12 (C–H), 13.93 (C–H); Anal. Calc. for $C_9H_{16}N_2O_2S$: C: 49.98%; H: 7.46%; N: 12.95%; S: 14.82%; Found: C: 49.89%; H: 7.53%; N: 12.91%; S: 14.85%.

N-Pentanoylmorpholine-4-carbothioamide (5h)

Mol. Wt. 230.33, Yield 77%, $R_f = 0.50$ (pet-ether: ethyl acetate 4:1), m.p 260 °C, Light yellow powder, IR (ATR, cm^{-1}) ν: 3359.75 (NH), 3059.25 (sp^2 C–H), 2974.30, 2865.51 (sp^3 C–H), 1713.74 (NCO stretch), 1564.12, 1479.88 (–C–H Bending), 1460.62 (C–N), 1434.67 (–C–H Bending), 1232.92 (C=S); ^{1}H NMR ($CDCl_3$): $\delta = 8.30$ (b, s, 1H, NH), 4.15 (b, s, 2H, O–CH_2), 3.80 (b, s, 4H, N–CH_2, O–CH_2), 3.69 (b, s, 2H, N–CH_2), 2.17 (t, 2H, $J = 7.50$ Hz, C–H), 1.63 (m, 4H, C–H), 0.94 (t, 3H, $J = 7.50$ Hz, C–H); ^{13}C NMR ($CDCl_3$): $\delta = 180.47$ (C=S), 175.47 (C=O), 66.20 (O–CH_2), 52.72 (b, N–CH_2), 51.64 (b, N–CH_2), 38.44 (C–H), 19.12 (C–H), 13.93 (C–H); Anal. Calc. for $C_{12}H_{22}N_2OS$: C: 52.15%; H: 7.88%; N: 12.16%; S: 13.92%; Found: C: 52.08%; H: 7.96%; N: 12.15%; S: 13.96%.

N-(2-Phenylacetyl)morpholine-4-carbothioamide (5i)

Mol. Wt. 264.36, Yield 75%, $R_f = 0.51$ (pet-ether: ethyl acetate 4:1), m.p 231 °C, Light yellow powder, IR (ATR, cm^{-1}) ν: 3104.90 (b, s 1H, NH), 2963.05 (sp^2 C–H), 2950, 2856.13 (sp^3 C–H), 1605.59 (NCO), 1538.83, 1549.20, 1495.68 (Ar–C=C), 1450.85 (–C–H bending), 1354.07 (–C–H bending), 1229.08 (C=S); ^{1}H NMR ($CDCl_3$): $\delta = 8.29$ (b, s, 1H, NH), 7.19 (t, 2H, $J = 8.2$ Hz, Ar–H), 7.08 (t, 1H, $J = 8.2$ Hz, Ar–H), 7.06 (d, 2H, $J = 8.2$ Hz, Ar–H), 4.20 (b, s, 2H, O–CH_2), 3.84 (b, s, 4H, N–CH_2, O–CH_2), 3.73 (b, s, 2H, N–CH_2), 3.47 (s, 2H, C–H); ^{13}C NMR ($CDCl_3$): $\delta = 180.93$ (C=S), 172.63 (C=O), 135.77 (Ar), 129.73 (Ar), 129.33 (Ar), 127.84 (Ar), 66.18 (O–CH_2), 52.60 (b, N–CH_2), 51.58 (b, N–CH_2), 40.53 (C–H); Anal. Calc. for $C_{13}H_{16}N_2O_2S$: C: 59.07%; H: 6.10%; N: 10.60%; S: 12.13%; Found: C: 59.0%; H: 6.18%; N:10.63%; S: 12.19.

N-Heptanoylmorpholine-4-carbothioamide (5j)

Mol. Wt. 258.14, Yield 70%, $R_f = 0.54$ (pet-ether: ethyl acetate 4:1), m.p 93.20 °C, Yellow powder, IR (ATR, cm^{-1}) ν: 3267.60 (NH), 2914.88, 2849.45 (sp^3 C–H), 1669.13 (NCO), 1514.42, 1459.74 (–C–H Bending), 1430.18 (C–N), 1238.52 (C=S); ^{1}H NMR ($CDCl_3$): $\delta = 8.27$ (b, s, 1H, NH), 4.13 (b, s, 2H, O–CH_2), 3.80 (b, s, 4H, N–CH_2, O–CH_2), 3.70 (b, s, 2H, N–CH_2), 2.16 (t, 2H, $J = 7.50$ Hz, C–H), 1.80 (q, 2H, $J = 7.20$ Hz, C–H), 1.34 (m, 6H, C–H), 0.90 (t, 3H, $J = 7.50$ Hz, C–H); ^{13}C NMR ($CDCl_3$): $\delta = 180.93$ (C=S), 175.40 (C=O), 66.15 (O–CH_2), 52.50 (b, N–CH_2), 51.52 (b, N–CH_2), 36.44 (C–H), 31.96 (C–H), 28.90 (C–H), 26.23 (C–H), 22.63 (C–H), 14.73 (C–H); Anal. Calc. for $C_{12}H_{22}N_2O_2S$: C: 55.78%; H: 8.58%; N: 10.84%; S: 12.41%; Found: C: 55.71%; H: 8.88%; N: 10.37%; S: 11.73%.

In vitro antimicrobial assays

Antibacterial assay

The antibacterial potential of the synthesized *N*-acyl-morpholine-4-carbothioamide (**5a**–**5j**) derivatives was evaluated using agar disk diffusion method in a well-maintained sterile environment. Two gram-negative bacterial strains (*Escherichia coli* (ATCC25992) and *Pseudomonas aeruginosa* (ATCC-15442)) and three gram-positive bacterial strains (*Staphylococcus aureus* (ATCC-6538), *Bacillus subtilis* (ATCC-6633) and *Klebsiella pneumoniae* (ATCC-1705)) were cultured in a nutrient broth at 37 °C for 24 h. According to the test specification (1 × 106 CFU/mL), seeding density of the bacterial culture was adjusted. To prepare lawn on the nutrient agar plates, 50 µL of refreshed cultures was poured on the agar media and swapped. 7 µL of the test compound (with final concentration of 70 µg/disk) was poured on the sterile filter paper disks (5 mm) and placed on nutrient ager plates, respectively. DMSO and ampicillin were used as negative and positive controls, respectively. The assay was performed in duplicate, and the plates were incubated at 37 °C for 24 h. The antibacterial activity of the compounds was determined by measuring the diameter of

zones (mm) showing complete inhibition with the help of vernier caliper [34].

Antifungal assays

The antifungal potential of the synthesized *N*-acyl-morpholine-4-carbothioamide (**5a**–**5j**) derivatives against *Aspergillus flavus* (FCBP 0064), *Aspergillus niger* (FCBP 0198) and *Fusarium solani* (FCBP 0291) was assessed as reported elsewhere. Stock cultures of fungal strains were cultured on sterile plates containing SDA (20–25 mL) and then swabbed/streaked through cotton buds. For spore formation, the plates were incubated at 28 °C for 7 days. After incubation, fungal spores were taken, and spore suspension was made in 0.02% v/v sterile Tween 20 solution in distilled water. Finally, turbidity was modified as per McFarland 0.5 turbidity standard. Standard agar disk diffusion method was employed for the analysis of possible antifungal potential of the compounds. 100 µL volume of spore suspension was taken for each fungal strain from Tween 20 solution (0.02% v/v) and swabbed on separate petri plates containing sterile SDA media. Compounds (7 µL) were applied to the sterilized filter paper disks (5 mm) which were then retained on the seeded SDA plates. Paper disks of amphotericin B (5 µL) served as a positive control, while the disk soaked with DMSO (7 µL) acted as a negative control. For fungal growth, the plates were then incubated at 28 °C for 24–48 h. After incubation, each loaded disk with compounds and controls were observed for the appearance of zone of inhibition. The diameter of ZOI was measured by using a vernier caliper to the nearest mm [35].

Antioxidant assays

Free radical scavenging activity (FRSA)

Free radical scavenging activity of the synthesized *N*-acyl-morpholine-4-carbothioamide (**5a**–**5j**) derivatives was determined using 2,2-diphenyl 1-picrylhydrazyl (DPPH) assay. Briefly, an aliquot of 20 µl from test sample (4 mg/mL DMSO) was mixed with 180 µL of DPPH solution (9.20 mg/100 mL methanol) in a 96-well plate. After incubation at 37 °C for 30 min, the absorbance was measured at 515 nm using microplate reader. Free radical scavenging activity of the tested samples was calculated using the following formula

$$\%\ \text{Inhibition} = \frac{(\text{absorbance of the control} - \text{absorbance of the sample})}{\text{absorbance of the controle}} \times 100.$$

The assay was performed in triplicate. Ascorbic acid and DMSO were used as positive and negative controls, respectively. The IC_{50} was calculated by twofold serial dilution method [36].

Total antioxidant capacity (phosphomolybdenum assay)

Total antioxidant capacity of the synthesized *N*-acyl-morpholine-4-carbothioamide (**5a**–**5j**) derivatives was determined by using phosphomolybdenum assay as reported previously. A reagent solution (900 µL) comprising of 4 mM ammonium molybdate, 28 mM sodium phosphate and 0.6 M sulfuric acid was mixed with 100 µL of the test compound. The mixture was then incubated at 95 °C for 90 min, followed by cooling at room temperature. Absorbance was measured at 630 nm using a microplate reader. Ascorbic acid was used as a standard (positive control) and DMSO as blank (negative control). The test was performed in triplicate, and the resultant TAC was expressed as µg ascorbic acid equivalent per mg dry weight of the compound (µg AAE/mg compound) [37].

Total reducing power estimation

The reducing power/capacity of the synthesized *N*-acyl-morpholine-4-carbothioamide (**5a**–**5j**) derivatives was estimated following previously reported potassium ferricyanide colorimetric assay, but with slight modifications. The assay was performed by taking 200 µL of each sample, 250 µL each of 0.2 M phosphate buffer and 200 µL of 1% (w/v) potassium ferricyanide. The reaction mixture was then incubated at 50 °C for 20 min. After incubation, 200 µL of 10% (w/v) TCA solution was added to the mixture followed by centrifugation at 3000 rpm for 10 min. An aliquot of 150 µL was taken from the supernatant of each mixture and shifted to corresponding well in the microwell plate. Lastly, 50 µL 0.1% (w/v) ferricyanide solution was added to each well and absorbance was measured at 630 nm. Ascorbic acid was used as a positive standard, while DMSO was used as a negative control. The assay was performed in triplicate, and reducing power of the test samples was expressed as µg ascorbic acid equivalent (AAE) per mg dry weight of the compounds (µg AAE/mg compound) [37, 38].

Biocompatibility against human red blood cells (hRBCs)

To investigate the biocompatible nature of the synthesized *N*-acyl-morpholine-4-carbothioamide (**5a**–**5j**) derivatives against isolated human red blood cells (hRBCs), a hemolytic assay was performed by a previously established protocol with minor modification. Briefly, fresh blood of about 3 mL was collected from a healthy individual and dispensed into a sterile EDTA tube. 1 mL blood was centrifuged (10000 rpm for 10 min) for the separation of RBCs. The suspension was washed thrice with PBS via centrifugation (2000 rpm for

10 min). For the preparation of erythrocytes suspension in phosphate-buffered saline (PBS), 200 µL of the washed pelleted erythrocyte was added to 4.8 mL of PBS (pH: 7.4) followed by gentle shaking. In separate Eppendorf tubes, erythrocyte suspension (180 µL) and test 20 µL sample were gently mixed and incubated for 1 h at 35 °C. The mixture was the centrifuged at 2000 rpm for 10 min, and supernatant was collected. The hemoglobin release was monitored using microplate reader (BIOTEK) at 540 nm after dispensing the supernatant in the 96-well plate. Triton X-100 and distilled water were used as positive and negative controls, respectively. Results were calculated as percentage hemolysis induced by compounds calculated through the following equation [26]

$$\%\,\text{Hemolysis} = \left[\frac{\text{ABs} - \text{ABnc}}{\text{ABpc} - \text{ABnc}}\right] \times 10$$

where ABs is the absorbance of the tested sample and ABnc and ABpc depict absorbance of negative and positive controls, respectively.

Methods

Preparation of ligand files

Files of the ligand were prepared using building module of the Molecular Operating Environment (MOE-2018) program by Chemical Computing Group (CCG) [39]. The ligand's geometries were drawn in building panel of MOE and were optimized at a standard MMFF94 force field level, having 0.0001 kcal/mol energy gradient convergence criterion [40]. The optimized 3D geometries were saved for further studies in a molecular database (mdb) file.

Preparation of receptor

Receptor was prepared in three steps involving 3D protonation, energy optimization and identification of active site [41]. Crystal structure of RNA (PDB code: 1j7t) [42] was obtained from protein data bank. Complexes structures were edited in MOE by removing solvent molecules. Structure preparation module of MOE was used for 3D protonated receptors and energy optimization in a default mode. The active site was identified using LigX module of the MOE marked around the co-crystallized ligands for both the receptors as both the receptors contain cognate ligands. MOE-Dock module was used to dock the optimized ligands with the RNA, and 30 independent computations were performed in total for each ligand. The highest docking score conformation was selected for each ligand to study the interactions in detail. Through MOE ligand interaction software, the 2D docking pose of the ligand protein complex having the lowest energy was used to visualize the 2D ligand–protein interactions.

Molecular docking

The MOE-Dock module was used to dock the optimized ligands with the RNA. For this purpose, 30 total independent computations were carried out through MOE simulations. Among the docked conformations, the conformation with highest score for each ligand was studied in detail. The lowest energy docking pose predicted by MOE program for the ligand–RNA complex was analyzed to visualize the 2D ligand–protein interaction.

Drug likeness

This study was performed using descriptor calculation module of the MOE 2018. The ligand property calculation function of MOE was used to perform the computations of the molecular descriptors for all the compounds (Table 6). Energy-minimized geometries of compounds **5a**–**5j** stored in molecular database (mdb) file of the MOE software were used to calculate the selected descriptors by using the descriptor calculation module of the MOE program.

Acknowledgements The author Mr. Hamid Aziz is highly grateful to the Higher Education Commission (HEC), Pakistan, for providing indigenous scholarship as the financial support for the research work performed.

Compliance with ethical standards

Conflict of interest All authors declare that they have no conflict of interest.

References

1. Nikaido H (2009) Multidrug resistance in bacteria. Ann Rev Biochem 78:119–146
2. Ascioglu S, Rex JH, De Pauw B, Bennett JE, Bille J, Crokaert F, Fiere D (2002) Defining opportunistic invasive fungal infections in immunocompromised patients with cancer and hematopoietic stem cell transplants: an international consensus. Clin Infect Dis 34(1):7–14
3. Moneer AA, Abouzid KAM, Said MM (2002) Synthesis of certain thiopyrimidine derivatives as antimicrobial agents. Az J Pharm Sci 30:150–160
4. Suhas R, Chandrashekar S, Gowda DC (2012) Synthesis of uriedo and thiouriedo derivatives of peptide conjugated heterocycles—a new class of promising antimicrobials. Eur J Med Chem 48:179–191
5. Suresha GP, Suhas R, Kapfo W, Gowda DC (2011) Urea/thiourea derivatives of quinazolinone–lysine conjugates: synthesis and structure–activity relationships of a new series of antimicrobials. Eur J Med Chem 46(6):2530–2540

6. Tuncel ST, Gunal SE, Ekizoglu M, Kelekci NG, Erdem SS, Bulak E, Dogan I (2019) Thioureas and their cyclized derivatives: synthesis, conformational analysis and antimicrobial evaluation. J Mol Struct 1179:40–56
7. Bielenica A, Stefańska J, Stępień K, Napiórkowska A, Augustynowicz-Kopeć E, Sanna G, Struga M (2015) Synthesis, cytotoxicity and antimicrobial activity of thiourea derivatives incorporating 3-(trifluoromethyl) phenyl moiety. Eur J Med Chem 101:111–125
8. Saeed A, Mustafa MN, Zain-ul-Abideen M, Shabir G, Erben MF, Flörke U (2019) Current developments in chemistry, coordination, structure and biological aspects of 1-(acyl/aroyl)-3-(substituted) thioureas: advances Continue…. J Sulfur Chem 40(3):312–350
9. Pingaew R, Prachayasittikul V, Anuwongcharoen N, Prachayasittikul S, Ruchirawat S, Prachayasittikul V (2018) Synthesis and molecular docking of *N*,*N*′-disubstituted thiourea derivatives as novel aromatase inhibitors. Bioorg Chem 79:171–178
10. Pérez H, O'Reilly B, Plutín AM, Martínez R, Durán R, Collado IG, Mascarenhas YP (2011) Synthesis, characterization, and crystal structure of Ni(II) and Cu(II) complexes with *N*-furoyl-*N*′,*N*′-diethylthiourea: antifungal activity. J Coord Chem 64(16):2890–2898
11. Saad FA, Buurma NJ, Amoroso AJ, Knight JC, Kariuki BM (2012) Co-ordination behaviour of a novel bisthiourea tripodal ligand: structural, spectroscopic and electrochemical properties of a series of transition metal complexes. Dalton Trans 41(15):4608–4617
12. Selvakumaran N, Ng SW, Tiekink ER, Karvembu R (2011) Versatile coordination behavior of *N*,*N*-di(alkyl/aryl)-*N*′-benzoylthiourea ligands: synthesis, crystal structure and cytotoxicity of palladium(II) complexes. Inorg Chim Acta 376(1):278–284
13. Phuong T, Khac-Minh T, Van Ha NT, Phuong HTN (2004) Synthesis and antifungal activities of phenylenedithioureas. Bioorg Med Chem Lett 14(3):653–656
14. Zhong Z, Xing R, Liu S, Wang L, Cai S, Li P (2008) Synthesis of acyl thiourea derivatives of chitosan and their antimicrobial activities in vitro. Carbohyd Res 343(3):566–570
15. Saeed A, Flörke U, Erben MF (2014) A review on the chemistry, coordination, structure and biological properties of 1-(acyl/aroyl)-3-(substituted) thioureas. J Sulfur Chem 35(3):318–355
16. Shah DR, Lakum HP, Chikhalia KH (2015) Synthesis and in vitro antimicrobial evaluation of piperazine substituted quinazoline-based thiourea/thiazolidinone/chalcone hybrids. Russ J Bioorg Chem 41(2):209–222
17. Keche AP, Kamble VM (2014) Synthesis and anti-inflammatory and antimicrobial activities of some novel 2-methylquinazolin-4 (3*H*)-one derivatives bearing urea, thiourea and sulphonamide functionalities. Arab J Chem 7(12):1522–1531
18. Abbas SY, El-Sharief MAS, Basyouni WM, Fakhr IM, El-Gammal EW (2013) Thiourea derivatives incorporating a hippuric acid moiety: synthesis and evaluation of antibacterial and antifungal activities. Eur J Med Chem 64:111–120
19. Erşen D, Ülger M, Mangelinckx S, Gemili M, Şahin E, Nural Y (2017) Synthesis and anti (myco) bacterial activity of novel 5,5-diphenylpyrrolidine *N*-aroylthiourea derivatives and a functionalized hexahydro-1*H*-pyrrolo[1,2-c]imidazole. Med Chem Res 26(9):2152–2160
20. Cui P, Li X, Zhu M, Wang B, Liu J, Chen H (2017) Design, synthesis and antibacterial activities of thiouracil derivatives containing acyl thiourea as SecA inhibitors. Bioorg Med Chem Lett 27(10):2234–2237
21. Uckun FM, Pendergrass S, Maher D, Zhu D, Tuel-Ahlgren L, Mao C, Venkatachalam TK (1999) *N*′-[2-(2-Thiophene) ethyl]-*N*′-[2-(5-bromopyridyl)] thiourea as a potent inhibitor of NNI-resistant and multidrug-resistant human immunodeficiency virus-1. Bioorg Med Chem Lett 9(24):3411–3416
22. Qasim M, Abideen Z, Adnan MY, Gulzar S, Gul B, Rasheed M, Khan MA (2017) Antioxidant properties, phenolic composition, bioactive compounds and nutritive value of medicinal halophytes commonly used as herbal teas. South Afr J Bot 110:240–250
23. Shon MY, Kim TH, Sung NJ (2003) Antioxidants and free radical scavenging activity of Phellinus baumii (Phellinus of Hymenochaetaceae) extracts. Food Chem 82(4):593–597
24. Zia-Ul-Haq M, Shahid SA, Ahmad S, Qayum M, Khan I (2012) Antioxidant potential of various parts of *Ferula assafoetida* L. J Med Plants Res 6(16):3254–3258
25. Evans BC, Nelson CE, Shann SY, Beavers KR, Kim AJ, Li H, Duvall CL (2013) Ex vivo red blood cell hemolysis assay for the evaluation of pH-responsive endosomolytic agents for cytosolic delivery of biomacromolecular drugs. J Vis Exp 73:e50166
26. Amin K, Dannenfelser RM (2006) In vitro hemolysis: guidance for the pharmaceutical scientist. J Pharma Sci 95(6):1173–1176
27. Pisano MB, Kumar A, Medda R, Gatto G, Pal R, Fais A, Era B, Cosentino S, Uriarte E, Santana L, Pintus F, Matos MJ (2019) Antibacterial activity and molecular docking studies of a selected series of hydroxy-3-arylcoumarins. Molecules 24(15):2815
28. Mendoza-Figueroa HL, Serrano-Alva MT, Aparicio-Ozores G, Martínez-Gudiño G, Suárez-Castillo OR, Pérez-Rojas NA, Morales-Ríos MS (2018) Synthesis, antimicrobial activity, and molecular docking study of fluorine-substituted indole-based imidazolines. Med Chem Res 27:1624
29. Liu JS, Deng LJ, Tian HY, Ruan ZX, Cao HH, Ye WC, Yu ZL (2019) Anti-tumor effects and 3D-quantitative structure–activity relationship analysis of bufadienolides from toad venom. Fitoterapia 134:362–371
30. Ruan ZX, Huangfu DS, Sun PH, Chen WM (2013) Molecular modeling studies on 3,4-dihydroquinazolines as trypanothione reductase inhibitors using 3D-QSAR and docking approaches. Med Chem Res 22(8):3541–3555
31. Ruan ZX, Huangfu DS, Xu XJ, Sun PH, Chen WM (2013) 3D-QSAR and molecular docking for the discovery of ketolide derivatives. Exp Opin Drug Disc 8(4):427–444
32. Lipinski CA, Lombardo F, Dominy BW, Feeney PJ (1997) Experimental and computational approaches to estimate solubility and permeability in drug discovery and development settings. Adv Drug Deliv Rev 23(1–3):3–25
33. Veber DF, Johnson SR, Cheng HY, Smith BR, Ward KW, Kopple KD (2002) Molecular properties that influence the oral bioavailability of drug candidates. J Med Chem 45(12):2615–2623
34. Jamil M, ul Haq I, Mirza B, Qayyum M (2012) Isolation of antibacterial compounds from *Quercus dilatata* L. through bioassay guided fractionation. Ann Clin Microb Antimicrob 11(1):11
35. Ahmed M, Fatima H, Qasim M, Gul B (2017) Polarity directed optimization of phytochemical and in vitro biological potential of an indigenous folklore: *Quercus dilatata* Lindl. ex Royle. BMC Comp Altern Med 17(1):386
36. Brand-Williams W, Cuvelier ME, Berset CLWT (1995) Use of a free radical method to evaluate antioxidant activity. LWT Food Sci Technol 28(1):25–30
37. Umamaheswari M, Chatterjee TK (2008) In vitro antioxidant activities of the fractions of *Coccinia grandis* L. leaf extract. Afr J Trad Comp Altern Med 5(1):61–73
38. Siddhuraju P, Mohan PS, Becker K (2002) Studies on the antioxidant activity of Indian Laburnum (*Cassia fistula* L.): a preliminary assessment of crude extracts from stem bark, leaves, flowers and fruit pulp. Food Chem 79(1):61–67
39. Molecular Operating Environment, 2015.08 (2015) Chemical Computing Group Inc., 1010 Sherbooke St. West, Suite 910, Montreal, QC, Canada, H3A 2R7

40. Halgren TA, Nachbar RB (1996) Merck molecular force field. IV. Conformational energies and geometries for MMFF94. J Comput Chem 17(5–6):587–615
41. Vicens Q, Westhof E (2001) Crystal structure of paromomycin docked into the eubacterial ribosomal decoding A site. Structure 9(8):647–658
42. Menozzi G, Merello L, Fossa P, Schenone S, Ranise A, Mosti L, La Colla P (2004) Synthesis, antimicrobial activity and molecular modeling studies of halogenated 4-[1*H*-imidazol-1-yl(phenyl) methyl]-1,5-diphenyl-1*H*-pyrazoles. Bioorg Med Chem 12(20):5465–5483

Affiliations

Hamid Aziz[1] · Aamer Saeed[1] · Muhammad Aslam Khan[2] · Shakeeb Afridi[2] · Farukh Jabeen[3,4]

✉ Hamid Aziz
hamidazizwazir@gmail.com

[1] Department of Chemistry, Quaid-I-Azam University, Islamabad 45320, Pakistan

[2] Department of Biotechnology, Quaid-I-Azam University, Islamabad 45320, Pakistan

[3] Department of Biology, Laurentian University, 935 Ramsey Lake Road, Sudbury, ON P3E 2C6, Canada

[4] Computation, Science, Research and Development Organization, 1401, 2485 Hurontario Street, Mississauga, ON L5A2G6, Canada